Journal of Zhejiang University-SCIENCE A 2026 27(6):583-597
www.jzus.zju.edu.cn; www.springer.com/journal/11582
E-mail: jzus_a@zju.edu.cn

Research Article
https://doi.org/10.1631/jzus.A2500404

Check for updates

Two-stage two-dimensional force allocation strategy for tunnel boring machines based on a region-reconfigurable thrust system

Zhe ZHENG[1], Kaihao ZHU[1], Jiaqi HOU[1], Haibo XIE[1], Lijie JIANG[2], Fulong LIN[2], Lianhui JIA[2], Laikuang LIN[3], Huayong YANG[1], Dong HAN[1]✉

[1]*State Key Laboratory of Fluid Power and Mechatronic Systems, School of Mechanical Engineering, Zhejiang University, Hangzhou 310058, China*
[2]*China Railway Engineering Equipment Group Co., Ltd., Zhengzhou 450047, China*
[3]*College of Mechanical and Electrical Engineering, Central South University, Changsha 410083, China*

Abstract: Determining the group forces of the thrust system is essential for trajectory control of tunnel boring machines (TBMs). Existing methods for selecting an optimal solution mainly consider the force variance among groups, while ignoring other constraints, such as uneven segment loading and excessive hydraulic shock. In this study, we develop a more comprehensive and robust framework for force allocation. First, a novel region-reconfigurable hydraulic system is designed, which enforces consistency among the forces acting on each segment. Then on this basis, for the ramping-up tunneling stage, quadratic programming (QP) is used to optimize force uniformity across the spatial dimension. Compared to the on-site allocation result, the improvement in force uniformity reaches up to 32.89%. Moreover, to address the hydraulic shock caused by excessive adjustment to the force, hydraulic compliance is introduced and optimized together with force uniformity using the non-dominated sorting genetic algorithm II (NSGA-II), which outperforms weighted QP by 1.25×10^6 kN^2 in uniformity and 2.86 kN^2 in compliance. Analyzing performance in the steady tunneling stage, the service life of the components improves significantly. To avoid a non-existent solution for the thrust force vector, a genetic algorithm-based error tolerance method is developed. Therefore, all deviation rectification commands can be answered with a minor compromise of up to 3% in the fitting accuracy of the thrust force vector. In summary, this framework enhances the adaptability and robustness of the force allocation strategy, providing a reliable foundation for TBM trajectory control.

Key words: Tunnel boring machine (TBM); Thrust system; Thrust force vector; Force allocation; Quadratic programming (QP); Non-dominated sorting genetic algorithm II (NSGA-II)

1 Introduction

Tunnel boring machines (TBMs) have excellent safety, efficiency, environmental compatibility, and automation control, which has led to their widespread use in tunnel construction (Zhang et al., 2020, 2024). As a crucial component of TBMs, the thrust system provides the momentum and force necessary to move the actual tunneling axis (ATA) in the direction of the desired tunneling axis (DTA) (Wang et al., 2022; Zheng et al., 2024). Nonetheless, TBMs are constantly exposed to varied and intricate stratigraphy, which creates uneven resistance (Chen and Yang, 2017; Wang, 2017). There is always a discrepancy between ATA and DTA, in addition to altitude measurement errors and control accuracy limits (Tang et al., 2022; Kong et al., 2024). A hierarchical control system, which involves a sequence of perception, recognition, decision-making, coordination, and execution, is a workable solution to this issue. TBM-Smart (Li et al., 2023a, 2023b), shield automatic intelligent control system (SHIELD_AICS) (Hu et al., 2022; SASAC, 2023), autonomous TBM (A-TBM) (MMC-Gamuda Tunnelling Training Academy, 2020), and other intelligent control systems have made extensive use of this approach.

Recognition and decision-making layers have employed a variety of machine learning techniques to ascertain macro-control instructions for the thrust system, such as instructions for the total advancing force,

✉ Dong HAN, dong_han@zju.edu.cn
Dong HAN, https://orcid.org/0000-0003-3292-979X

Received Aug. 27, 2025; Revision accepted Dec. 14, 2025;
Crosschecked Mar. 6, 2026; Online first May 20, 2026

© Zhejiang University Press 2026

advancing speed, and penetration rate, based on the TBM state and geological conditions required by the perception layer (Xu et al., 2019; Harandizadeh et al., 2021; Li et al., 2021). Multiple hydraulic cylinders make up the thrust system, which involves multiple-input multiple-output features (Wang et al., 2022; Zheng et al., 2024). These instructions are then broken down into reference signals for each hydraulic cylinder by the coordination layer. Lastly, to guarantee that the reference signals can be precisely tracked, a feedback-based controller is designed and used at the execution layer. Among these aforementioned techniques, this study focuses on the coordination layer.

Due to its underactuated characteristic, the thrust system only produces an advancing force, pitching moment, and yawing moment, which is also known as the thrust force vector (Zhu et al., 2023). However, there are more inputs than outputs (Liu and Shao, 2010). In other words, this is an underdetermined system that has infinite possible input combinations given a preset thrust force vector. Numerous studies have looked for a solution to this issue.

One crucial assumption of force allocation is the quasi-static behavior of the TBM. Quasi-static refers to a situation where the state variables of a system evolve so slowly that it remains almost in equilibrium, though not being strictly static or perfectly constant. TBM tunneling is a process with high inertia and long delay, with an advance speed typically about 10–20 mm/min; this can be regarded as a slow transition between a series of near-equilibrium states. On this basis, Wang et al. (2022) created a universal inverse statics equation using the thrust system's velocity Jacobian matrix and virtual work. Based on this, a solution was found using the Moore–Penrose pseudoinverse method. Another method is to make each hydraulic cylinder's force increase linearly from top to bottom (Zhu et al., 2021). Even though these techniques can produce a combination of inputs, they fail to account for force uniformity—the variation in pressure between groups. Since the lining segments directly bear the reaction force of the hydraulic cylinder (Dai et al., 2022), the composite stratum may experience significant eccentric loading (Chen and Mo, 2009; Deng et al., 2015; Yang et al., 2018; Shi et al., 2022), raising the possibility of segment damage and cracking, and ultimately compromising the structural durability and safety of the tunnel.

To address this issue, Deng et al. (2011a, 2011b, 2015) developed static force transmission equations for the thrust system, adding force uniformity as a requirement. Adequate segment protection under large eccentric loads was enabled through the optimal solution found using the Lagrange multiplier method. Some researchers have updated the thrust system's hydraulic cylinder configurations based on this framework. For instance, Deng et al. (2019, 2021) improved anti-eccentric load capabilities by creating various non-uniform hydraulic cylinder layouts. Also, the force-on-off principle, as proposed by Guo et al. (2018), dynamically decides whether or not a hydraulic cylinder in the thrust system should produce force. Using force uniformity, an exhaustive search is conducted to determine the best principle. As another example, Guo and Guo (2017) proposed a self-adaptive thrust system that could allocate any hydraulic cylinder to the groups that were next to it. A thorough search was also conducted to determine the optimal solution for this approach.

Overall, while the aforementioned research has improved our understanding of force uniformity, there are still specific issues that need to be resolved:

(1) The only factor accounted for is force uniformity among the groups. The hydraulic cylinders operating on the same segment, however, can belong to different groups. Consequently, each segment may experience a local force eccentricity, which is particularly severe in these proposed thrust systems.

(2) Excessive force adjustment brought on by uneven strata is another issue. In this situation, the segments and hydraulic components may experience pressure shock. Reducing the variation in each thrust force vector adjustment as much as possible is a more efficient solution than the conventional passive pressure absorbance method (Shi et al., 2013). As a result, it is also necessary to minimize the force difference between each group. However, the force allocation studies mentioned above did not examine this restriction.

(3) The Moore–Penrose pseudoinverse method is often used to obtain a solution. However, the limits of the group force's boundary are typically disregarded with this approach. Stated differently, the stability and convergence of the solvers have not been thoroughly demonstrated. Furthermore, under some severe working conditions encountered during long-term TBM operation, there may not be a feasible solution for group force. This issue has not been addressed in previous research.

In addition to the aforementioned hierarchical control framework, many researchers have used reinforcement learning (RL) to forecast each group's force based

on geological conditions and TBM states, omitting the force allocation process (Jia et al., 2023; Xu et al., 2023; Elbaz et al., 2024; Lin et al., 2024). Because the TBM excavation process is treated as a black box in these investigations, nonlinear dynamics that are not considered by the quasi-static assumption can be included. Theoretically, the force of each group is more flexible. Nevertheless, hydraulic compliance and force uniformity are not regarded as reward functions. At the same time, RL's convergence and resilience are inferior to those of hierarchical frameworks due to weak generalizability. A summary of the related studies is provided in Table 1.

Motivated by the aforementioned considerations, a novel two-stage two-dimensional force allocation (TS2DFA) strategy based on a region-reconfigurable thrust system is proposed. Our study makes the following contributions:

(1) A novel thrust hydraulic system is created that has fixed grouping but movable spatial regions. Multiple solenoid directional valves are used to construct this setup, allowing for real-time customization. This leads to one-to-one relationships between the ring segments and force groups.

(2) A performance metric is specifically designed for force allocation. In the spatial domain, the force uniformity is used to assess the distribution of forces around the segment linings. The hydraulic compliance is used to lessen the amplitude of force fluctuations in the temporal domain. Therefore, the suggested framework represents a multi-objective multi-dimensional optimization of the force allocation.

(3) Because the shield tunneling process is tiered, we only consider force uniformity during the ramping-up stage, and quadratic programming (QP) is used to solve the force allocation problem. Both force uniformity and hydraulic compliance are considered during the steady tunneling stage, and the non-dominated sorting genetic algorithm II (NSGA-II) is used to obtain the best solution. Moreover, in the case where there is no feasible solution in the local confined space, an over-constrained solver is proposed. As a result, all deviation rectification commands can be answered with a small compromise in the fitting accuracy of the thrust force vector.

2 Research significance

As listed in Table 1, existing studies on force allocation have left some research gaps. This paper presents a novel framework that outperforms conventional methods, mainly in the following areas:

(1) Current fixed-grouped thrust systems and some variations can optimize the force uniformity that characterizes the entire lining segments. However, they neglect how forces from several groups can apply to the same segment. Our proposed region-reconfigurable thrust system is a low-cost retrofitting method that solves this issue at the hydraulic system level.

(2) Current force planning algorithms concentrate solely on the uniformity of force across segments and do not consider the constraints on pressure change. In addition to producing hydraulic shock, a significant pressure change can also greatly increase the pressure stabilization period. In this study, we account for both force uniformity and hydraulic compliance, and construct a novel optimization framework that fits the cyclic nature of a TBM.

(3) Most current methods cannot deal with cases where the feasible set is empty. We propose a novel error-tolerance solver that only slightly compromises

Table 1 Comparison of force allocation strategies

Study	Group number	Configuration	Constraint	Non-solution	Solver
Wang et al. (2022)	4	Fixed	–	Yes	Virtual work
Zhu et al. (2021)	6	Fixed	–	Yes	Linear distribution
Deng et al. (2011b)	4	Fixed	Uniformity	Yes	Lagrange multiplier
Deng et al. (2021)	4	Non-uniform	Uniformity	Yes	Lagrange multiplier
Guo et al. (2018)	4	Force-on-off	Uniformity	Yes	Lagrange multiplier
Guo and Guo (2017)	4	Self-adaptive	Uniformity	Yes	Virtual work
Shi et al. (2013)	4	Fixed	Compliance	Yes	–
Elbaz et al. (2024)	4	Fixed	–	Yes	RL
Our work	10	Region-configurable	Uniformity and compliance	No	QP, NSGA-II, and LLS

QP: quadratic programming; NSGA-II: non-dominated sorting genetic algorithm II; LLS: linear least squares

the reconstruction accuracy of the thrust force vector and provides an alternative solution near the boundary of the feasible space, ensuring that each commanded thrust force vector can be executed.

3 Design of the region-reconfigurable thrust system

As our study subject, the excavation diameter of the "Linghang" TBM, which is utilized in the Chongtai Yangtze River Tunnel, is 15.4 m. To lower the system cost and complexity of control, the hydraulic cylinders of the thrust system are separated into six groups. All hydraulic cylinders within the same group are controlled by the proportional pressure-reducing valve (PPRV). Ten segments make up a whole lining segment: two adjacent segments (L1 and L2), seven standard segments (B1–B7), and one key segment (K). The K segment's location in each ring needs to be offset by a specific angle to provide attitude correction and enable staggered installation. To prevent insertion interference and possible damage during assembly, the K segment may be positioned anywhere around the tunnel, except for the 45° area at the bottom of the tunnel (Gong et al., 2024). For illustrative purposes, in this section, we consider the case where the K segment is located on hydraulic cylinders 1 and 28. During tunneling, due to factors such as geological heterogeneity and shield steering, significant pressure differentials frequently occur among these groups.

As seen in Fig. 1a, the hydraulic cylinders acting on segment L1 are part of groups A and B, and they output different forces. L1 experiences an overturning moment because of this pressure differential. This phenomenon also occurs in the adjacent segment L2, as well as the standard segments B3 and B5. Similarly, as illustrated in Fig. 1b, the overturning moment is observed when the K segment is located at hydraulic cylinder 1. The primary reason for this is that the segments' spatial locations change while the group's spatial arrangement remains constant throughout time. As a result, the overturning moments inevitably remain throughout the tunneling process and cannot be eliminated. This persistent imbalance easily leads to localized crushing of individual segments, which in turn impacts the structural quality and service life of the lining segments.

The key to designing a novel thrust system that eliminates the overturning moment is to satisfy two requirements simultaneously: (1) one-to-one matching between the number of segments and groups and (2) real-time alignment of group locations with the spatial positions of the segments. A novel thrust hydraulic system that is region-adjustable but group-fixed is accordingly proposed for the "Linghang" TBM, as illustrated in Fig. 2. The key characteristic of this system is that the number of thrust groups is determined

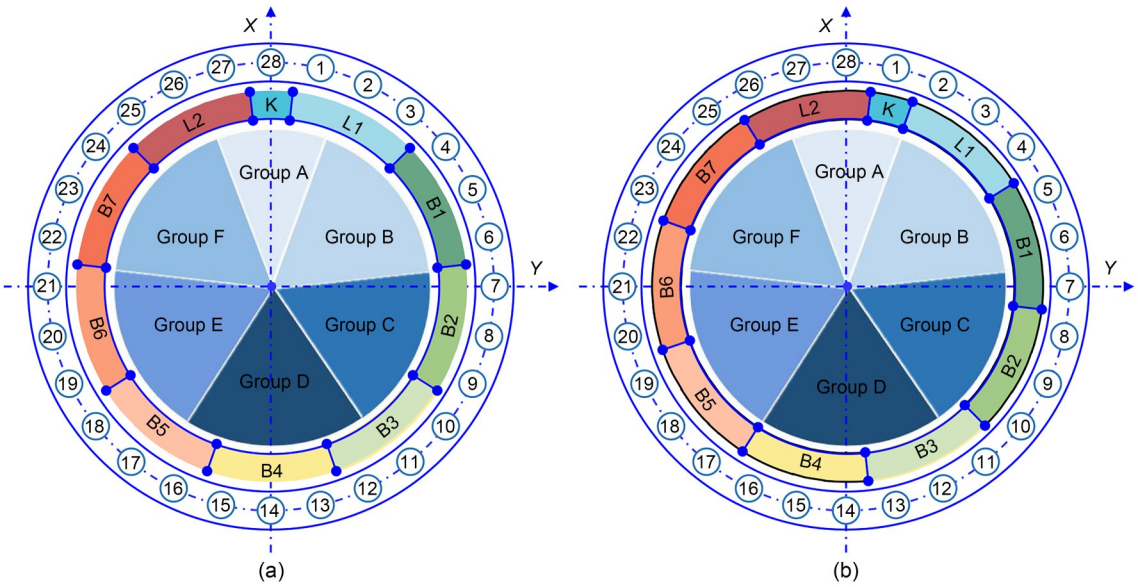

Fig. 1 Group layout of the fixed thrust system: (a) K segment located at hydraulic cylinder 28; (b) K segment located at hydraulic cylinder 1. 1–28: hydraulic cylinder; K, L1 and L2, and B1–B7: segment; A–F: group

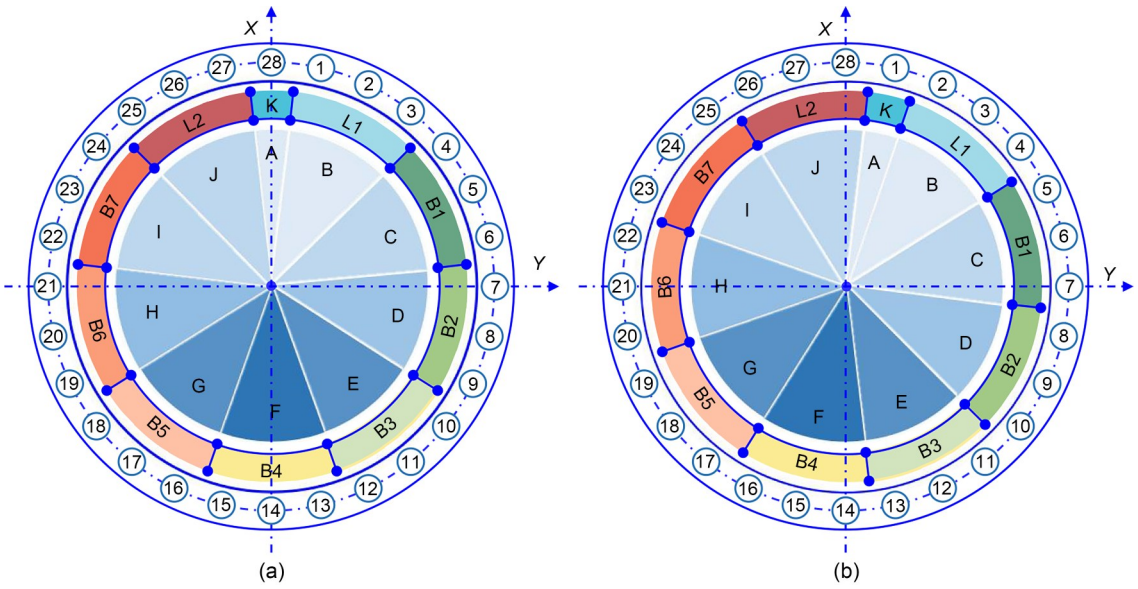

Fig. 2 Group layout of the region-reconfigurable thrust system: (a) K segment located at hydraulic cylinder 28; (b) K segment located at hydraulic cylinder 1. 1–28: hydraulic cylinder; K, L1 and L2, and B1–B7: segment; A–J: group

by the number of segments in a ring. Consequently, the thrust system is divided into 10 groups to guarantee that the force exerted by the hydraulic cylinders on each segment remains uniform. In this regard, each hydraulic cylinder can work in one of the following four modes: as an independent group, grouped with the two cylinders on its left, grouped with its two neighboring cylinders, or grouped with the two cylinders on its right. To implement this region-reconfigurable concept, a novel hydraulic system that comprises 11 PPRVs and 43 two-position three-way solenoid directional valves (TTSDVs) is proposed; its details are provided in Section S1 of the electronic supplementary materials (ESM).

4 Framework of force allocation based on the region-reconfigurable thrust system

As previously mentioned, the load operating on the TBM is represented as a 6D vector [F_x, F_y, F_z, M_x, M_y, M_z], where F_x, F_y, and F_z denote the forces along the x-, y-, and z-axes, respectively, and M_x, M_y, and M_z denote the moments about the x-, y-, and z-axes, respectively. The thrust system cannot directly generate the force vectors perpendicular to the tunneling axis due to its under-actuated characteristics. Consequently, the translational movements along the x- and y-axes are not actively regulated. Additionally, the variable loads of the thrust system are restricted to F_z, M_x, and M_y, as the torque around the z-axis is usually changed through cutterhead reversal. For clarity, the subsequent study is conducted using the layout in Fig. 2a. The static equilibrium equations of the thrust system are stated as:

$$\begin{cases} \sum_{k=1}^{10} n_k F_k - F_z = 0, \\ \sum_{k=1}^{10} a_k F_k - \dfrac{M_x}{r} = 0, \\ \sum_{k=1}^{10} b_k F_k + \dfrac{M_y}{r} = 0, \end{cases} \tag{1}$$

$$\begin{aligned} a_k &= \sum_{k=1+n_{k-1}!}^{n_k!} \sin\left[\theta_0 - \frac{2\pi}{N}(k-1)\right], \\ b_k &= \sum_{k=1+n_{k-1}!}^{n_k!} \cos\left[\theta_0 - \frac{2\pi}{N}(k-1)\right], \end{aligned} \tag{2}$$

where N is the number of hydraulic cylinders, n_k is the number of hydraulic cylinders in the kth group, r is the installation radius of the hydraulic cylinders, F_k is the thrust of the kth group, a_k and b_k are the sums of the sine and cosine values of the hydraulic cylinders in the kth group with respect to the x- and y-axes, respectively, and θ_0 is the angle between hydraulic cylinder 1 and the x-axis.

As stated in Zheng et al. (2024), TBM operation, being a complex human-in-the-loop autonomous control system, naturally exhibits a hierarchical architecture

and follows the principle of increasing precision from higher to lower levels. The upper-level layer focuses on slowly varying behaviors, such as attitude variation, while the lower-level layer handles fast dynamic loops, such as pressure and speed control. In other words, the nonlinear behaviors of the hydraulic system (such as valve hysteresis, fluid compressibility, and model uncertainties) should be considered at the execution level (Wang et al., 2022). Moreover, under the assumption of quasi-static behavior, the desired steady-state pressure of the hydraulic cylinders is of greater concern than the transient dynamics. In related studies on force allocation (Deng et al., 2015; Guo and Guo, 2017; Gou et al., 2018; Wang et al., 2022), hydraulic properties have generally not been modeled explicitly. To address potential issues such as long adjustment times or tracking errors caused by limited control performance, we update the thrust force vector and the corresponding group force based on the latest measured attitude deviations. In Zhang et al. (2022), the decision-making and the feedback controllers were operated at 1 and 100 Hz, respectively, so that the high-level command had sufficient time to converge. Therefore, even without explicit modeling of the nonlinear hydraulic properties, the high-level controller can ensure a gradual convergence of the actual tunneling trajectory.

4.1 Optimization objectives for force allocation

Since the number of equations (which correspond to the controllable degrees of freedom of the TBM) is much less than the number of variables, the linear system defined by Eq. (1) is underdetermined. In theory, there are an endless number of solutions to this system; however, in practice, each group is subject to precise limits on its force output. As a result, the intersection between the feasible region (which is commonly described as a positive orthotope) and the theoretical solution space (an affine subspace) is severely constrained. Furthermore, an incorrect configuration of the group forces may fail to precisely recreate the required thrust vector, as well as lead to some undesired outcomes, such as internal force interference and unequal segment loading within the thrust system. The thrust allocation uniformity (J_{TAU}) constraint is thus generated to address this issue, which optimizes the force variance along the circumferential spatial dimension. The segmental load imbalance is exacerbated by higher force variations as J_{TAU} grows, resulting in a substantial decrease in force distribution upon the segments. Therefore, it is imperative to reduce J_{TAU} during optimization, a process that can be expressed as:

$$J_{\mathrm{TAU}}=\frac{1}{10}\sum_{k=1}^{10}\left(F_k-\bar{F}\right)^2, \tag{3}$$

where $\bar{F}$ is the average force of the thrust system, given by:

$$\bar{F}=\frac{1}{10}\sum_{k=1}^{10}F_k. \tag{4}$$

During the tunneling operation, the desired thrust force vector changes frequently due to the uneven geology and steering requirements. Consequently, the hydraulic cylinders in each group are susceptible to abrupt pressure drops and surges, which induce instantaneous pressure shocks to the hydraulic components and segments. The compliance evaluation function C quantifies the compliance characteristic of the thrust system, which is denoted as:

$$C=\frac{\Delta F}{A\Delta p}, \tag{5}$$

where ΔF is the desired force change of the hydraulic cylinder, Δp is the pressure change, and A is the effective area of the hydraulic cylinder.

To minimize the pressure change Δp of each cylinder between two allocation steps, a thrust allocation compliance (J_{TAC}) is introduced:

$$J_{\mathrm{TAC}}=\sum_{k=1}^{10}\left[F_k(m)-F_k(m-1)\right]^2, \tag{6}$$

where $F_k(m-1)$ and $F_k(m)$ denote the forces of the hydraulic cylinder in the kth group at the $(m-1)$th and mth allocation steps, respectively.

One specific emphasis of J_{TAU} is the circumferential uniformity of the force applied to the entire lining segment. The gripper of the thrust hydraulic cylinders would work on a new set of segments after each tunneling cycle, significantly lowering the risk of segmental crushing and misalignment in the spatial dimension. In contrast, J_{TAC} is defined in the temporal domain, since it enhances the service life of hydraulic components by continuously limiting the pressure variations within the same set of hydraulic components. Therefore, we consider this force allocation strategy to be

not only a multi-objective optimization but also a spatiotemporal optimization framework. In practice, the tunneling process of a TBM can be divided into a ramping-up stage and a steady stage. The primary goal of the former stage is to quickly raise the total advancing force and transition the TBM to the steady stage. In particular, the working pressure of the hydraulic cylinders at the bottom of the thrust system is subjected to the fastest variation in order to offset the TBM's own weight. Once the force change is restricted at the ramping-up stage, the pressure rise can be slowed, which may result in the TBM pitching forward. Consequently, during the ramping-up stage, only J_{TAU} is accounted for, whereas during the steady stage, both J_{TAU} and J_{TAC} are included. To identify the ramping-up stage, we designate the breakpoint as the first point within the initial 1/3 of the entire excavation stage in which the signal surpasses the upper quartile.

4.2 Force allocation for the ramping-up stage

The objective function J_{TAU} is reformulated as:

$$\begin{aligned} J_{\mathrm{TAU}} &= \frac{1}{10}\left(\sum_{k=1}^{10}F_k^2 - 2\bar{F}\sum_{k=1}^{10}F_k + 10\bar{F}^2\right) \\ &= \frac{1}{10}\sum_{k=1}^{10}F_k^2 - \left(\frac{1}{10}\sum_{k=1}^{10}F_k\right)^2 \\ &= \frac{1}{10}\boldsymbol{x}^{\mathrm{T}}\boldsymbol{x} - \left(\frac{1}{10}\mathbf{1}^{\mathrm{T}}\boldsymbol{x}\right)^2, \end{aligned} \tag{7}$$

where $\boldsymbol{x}$ represents a vector composed of group forces and $\mathbf{1}\in\mathbb{R}^{10\times1}$ is a column vector of ones.

For any non-zero vector $\boldsymbol{z}=[z_1, z_2, \cdots, z_n]^{\mathrm{T}}\in\mathbb{R}^n$, consider that:

$$\begin{aligned} \boldsymbol{z}^{\mathrm{T}}\nabla^2\boldsymbol{z} &= \frac{2}{n}\boldsymbol{z}^{\mathrm{T}}\boldsymbol{z} - \frac{2}{n^2}\boldsymbol{z}^{\mathrm{T}}\mathbf{1}\mathbf{1}^{\mathrm{T}}\boldsymbol{z} \\ &= \frac{2}{n}\|\boldsymbol{z}\|^2 - \frac{2}{n^2}\left(\sum_{i=1}^{n}z_i\right)^2 \geqslant 0, \end{aligned} \tag{8}$$

where n denotes the dimension of vector $\boldsymbol{x}$ and z_i is the ith component of $\boldsymbol{z}$.

Owing to the positive semi-definite nature of the matrix $\boldsymbol{z}^{\mathrm{T}}\nabla^2\boldsymbol{z}$. The equality constraint defined in Eq. (1) is a typical convex optimization framework. Although some heuristic algorithms—such as the genetic algorithm (GA) and particle swarm optimization (PSO) algorithm—can conduct global searches of the solution space, they are more suitable for handling nonlinear or non-convex problems. The Lagrange multiplier, which is frequently employed in other studies, is restricted to optimization problems with unbounded variables that are confined by equality. With these factors in mind, the QP method is used to resolve the forces of each group while considering these parameters. As a result, the single-dimensional force allocation (SDFA) strategy is formulated, which includes a decision variable, an objective function, and an equality constraint. This technique is summarized as follows:

$$\begin{aligned} &\min_{x\in\mathbb{R}^{10}}\frac{1}{2}\boldsymbol{x}^{\mathrm{T}}\boldsymbol{Q}\boldsymbol{x}, \\ &\text{s.t.}\quad \boldsymbol{A}_{\mathrm{eq}}\boldsymbol{x}=\boldsymbol{b}_{\mathrm{eq}},\quad \boldsymbol{x}_{\min}\leqslant\boldsymbol{x}\leqslant\boldsymbol{x}_{\max}, \end{aligned} \tag{9}$$

$$\boldsymbol{A}_{\mathrm{eq}} = \begin{bmatrix} n_1 & n_2 & n_3 & \cdots & n_{10} \\ a_1 & a_2 & a_3 & \cdots & a_{10} \\ b_1 & b_2 & b_3 & \cdots & b_{10} \end{bmatrix}, \tag{10}$$

$$\boldsymbol{Q} = \frac{\boldsymbol{I}_{10}}{10} - \frac{\mathbf{1}_{10}}{100}, \tag{11}$$

$$\boldsymbol{b}_{\mathrm{eq}} = \begin{bmatrix} F_z & \dfrac{M_x}{r} & -\dfrac{M_y}{r} \end{bmatrix}^{\mathrm{T}}, \tag{12}$$

where $\boldsymbol{Q}$ is the Hessian matrix of the objective function J_{TAU}, $\boldsymbol{A}_{\mathrm{eq}}$ is the coefficient matrix relating the group forces to the resultant thrust vector, $\boldsymbol{b}_{\mathrm{eq}}$ is the target thrust vector, $\boldsymbol{I}_{10}\in\mathbb{R}^{10\times10}$ is the identity matrix, and $\mathbf{1}_{10}\in\mathbb{R}^{10\times10}$ is a matrix with all entries equal to one.

Next, consider the ramping-up stage of the 15th and 30th rings of the "Linghang" TBM, where the K segment is located at hydraulic cylinder 1. The related fixed-grouped and region-reconfigurable thrust systems are illustrated in Figs. 1b and 2b, respectively. Before analysis, data preprocessing must be implemented, which includes the identification of outliers through an isolation forest algorithm and denoising of data using a Savitzky–Golay filter. These approaches were implemented in our previous study and demonstrated a favorable impact on the management of noisy data (Zhang et al., 2022; Wang et al., 2024). With these processed data, two force allocation strategies are compared: the fixed-grouped thrust system-based SDFA (FSDFA) and the region-reconfigurable thrust system-based SDFA (RSDFA). The main parameters of the thrust system are listed in Table 2.

The findings are compared to on-site results, as shown in Figs. 3 and 4. FSDFA generates group forces that are more uniform than those that are manually allocated. In ring 15, J_{TAU} improves by an average of

Table 2 Main parameters of the thrust system

Parameter	Value
Number of cylinders in the thrust system, N	28
Number of cylinders in group A, n_1	1
Number of cylinders in groups B–J, n_2	3
Distribution radius of the cylinders, r (m)	7.75
Angle between cylinder 1 and the x-axis, θ_0	$\pi/28$

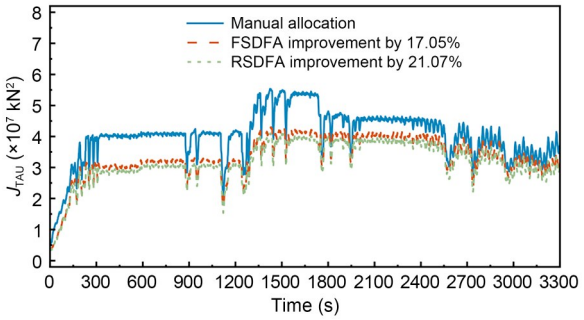

Fig. 3 Comparison of J_{TAU} in the ramping-up stage of ring 15

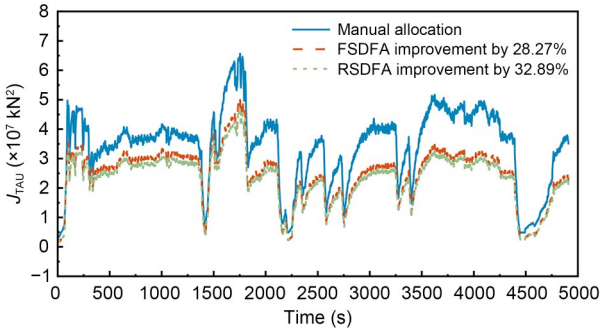

Fig. 4 Comparison of J_{TAU} in the ramping-up stage of ring 30

17.05%, while in ring 30, the improvement reaches 28.27%. This demonstrates that the group forces—which are chosen by the driver based on experience—are characterized by significant randomness. However, in some cases, they may offer a solution that is relatively close to the optimal global solution. In contrast, the solution produced using QP guarantees the discovery of a globally optimal solution in the feasible region, as specified by the linear constraints. Furthermore, RSDFA surpasses FSDFA, confirming that the region-reconfigurable approach enhances force uniformity. This enhancement is due to the increased dimensionality of the possible solution space, which allows for greater flexibility in force allocation.

Notably, J_{TAU} undergoes some step changes during the ramping-up stage. This is the result of the growing penetration rate of the TBM cutterhead system, which causes a quick increase in the thrust force vector and a concomitant surge in force variance within groups. Similar peaks and troughs are observed in J_{TAU} during the excavation. The energy accumulation and dissipation mechanism inherent in the rock-breaking process is responsible for these oscillations. The thrust force vector decreases following rock fracturing as a result of a decrease in the penetration rate.

4.3 Force allocation for the stable stage

To simultaneously consider J_{TAU} and J_{TAC} during the stable stage, they must be integrated into a single constraint using weighted summation because QP is a conventional single-objective optimization approach. Accordingly, a region-reconfigurable thrust system-based two-dimensional weighted force allocation (RTWFA) strategy is established. A typical quadratic form depicting the orthogonal projection of the prior thrust force vector can be rewritten as:

$$J_{TAC}=\sum_{k=1}^{10}[F_k(m)-F_k(m-1)]^2=\|\boldsymbol{x}-\boldsymbol{x}_{prev}\|^2, \quad (13)$$

where $\boldsymbol{x}_{prev}$ is the value of $\boldsymbol{x}$ at the previous allocation step.

This function is a quadratic function with a linear term, and its Hessian is:

$$\nabla^2 J_{TAC}=2\boldsymbol{I}_{10}. \quad (14)$$

Since Eqs. (8) and (14) are convex quadratic functions, provided α, $\beta\geqslant 0$, the synthesis function will remain convex, where α and β are the non-negative weighting coefficients of J_{TAU} and J_{TAC}, respectively. Therefore, the weighted objective function can be defined as:

$$\min_{\boldsymbol{x}\in\mathbb{R}^{10}}\frac{1}{2}\boldsymbol{x}^{\mathrm{T}}\boldsymbol{H}\boldsymbol{x}-\boldsymbol{x}_{prev}^{\mathrm{T}}\boldsymbol{x}, \quad (15)$$

$$\text{s.t.}\quad \boldsymbol{A}_{eq}\boldsymbol{x}=\boldsymbol{b}_{eq},\quad \boldsymbol{x}_{min}\leqslant\boldsymbol{x}\leqslant\boldsymbol{x}_{max},$$

$$\boldsymbol{H}=2(\alpha\boldsymbol{Q}+\beta\boldsymbol{I}_{10}), \quad (16)$$

where $\boldsymbol{H}$ is the Hessian matrix of the weighted objective function.

In the above formula, α, $\beta>0$, and $\alpha+\beta=1$. At this point, the eigenspace of the matrix $\alpha\boldsymbol{Q}+\beta\boldsymbol{I}_{10}$ is distinct from that of $\boldsymbol{Q}$ or $\boldsymbol{I}_{10}$ alone. In other words, the direction of its minimal eigenvector is a combination of the minimum eigenvectors of the two distinct constraints, which

suggests a shift in the best solution direction. A larger α indicates a greater emphasis on J_{TAU} in the force allocation, while a larger β suggests a preference for J_{TAC}, as per the concept of non-dominated Pareto solutions. Using the steady stage of ring 6 as an example, five different combinations C1–C5 of relative importance weights are shown in Table 3.

Table 3 Combinations of relative importance weights

Combination	α	β
C1	0.3	0.7
C2	0.4	0.6
C3	0.5	0.5
C4	0.6	0.4
C5	0.7	0.3

We take the C3 weight configuration as the baseline, with comparative results illustrated in Fig. 5. Compared to the manually assigned forces of each group, RTWFA shows better performance in terms of force uniformity and hydraulic compliance.

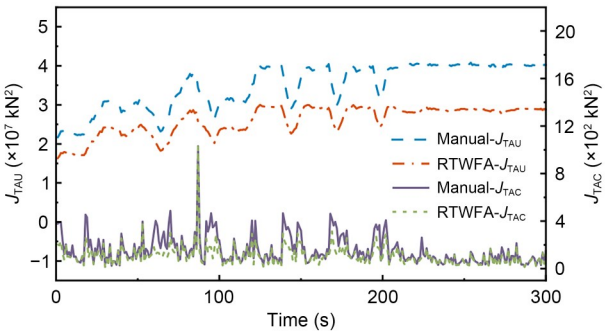

Fig. 5 Comparison of on-site results and RTWFA in the steady stage of ring 6

Fig. 6 illustrates a comparison of RTWFA performance under various weighting methods, with the C1 weight configuration serving as the baseline. The differences in values from C1 to C5 are all positive, indicating that J_{TAU} decreases gradually from C1 to C5. This suggests that the direction of $\boldsymbol{H}$ becomes closer to the vector $\boldsymbol{Q}$ as α increases, i.e., it moves toward the gradient that optimizes force uniformity.

In contrast, the sign of the differences in J_{TAC} itself is inconsistent; it is not globally monotonic, as it can be either positive or negative. For instance, the compliance value J_{TAC} for C5 is the smallest at the 7th allocation step, while the smallest compliance J_{TAC} occurs

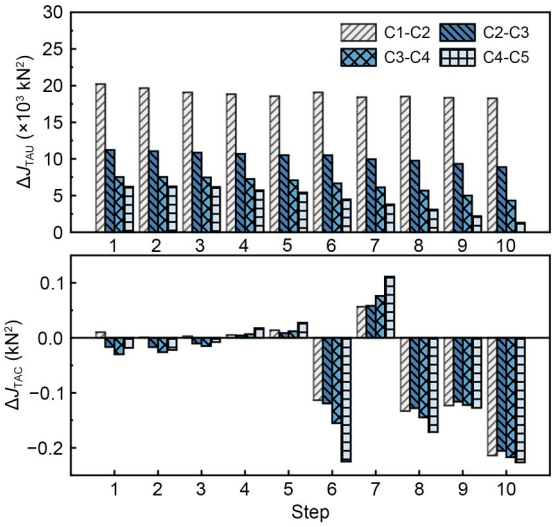

Fig. 6 Comparison of different weight coefficients

at C1 at the 6th allocation step. This behavior appears to be in direct opposition to the negative connection with β that we deduced from Eq. (16). The reason for this is that the magnitudes of the force uniformity and hydraulic compliance differ significantly. The gradient of the combined constraint $\alpha\boldsymbol{Q}+\beta\boldsymbol{I}_{10}$ can deviate from the intended direction within the 10D solution space when the constraint that $\alpha+\beta=1$ is satisfied.

In the first five allocation steps, the compliance discrepancies associated with each weight are minor (mostly below 0.05). This is because the changes in the thrust force vector are minimal during those steps, which means that the group force does not necessitate significant force adjustments. Beginning at step 6, however, J_{TAC} differences grow noticeably, demonstrating the strong coupling between hydraulic compliance and the magnitude of the thrust force vector change. Furthermore, although the J_{TAC} values are not monotonically decreasing, the cumulative J_{TAC} of C1 remains the smallest over the 10 steps. This phenomenon is consistent with the idea that compliance is influenced by time.

To overcome the limitations of manual weight assignment, NSGA-II is implemented to identify a Pareto-optimal solution set that simultaneously satisfies J_{TAU} and J_{TAC}. The details of the region-reconfigurable thrust system-based NSGA-II force allocation (RTNFA) strategy are provided in Section S2 of the ESM. A comparative analysis with RTWFA is presented in Fig. 7. The positive values of ΔJ_{TAU} across all cases indicate that the optimal solution selected by RTNFA from the Pareto

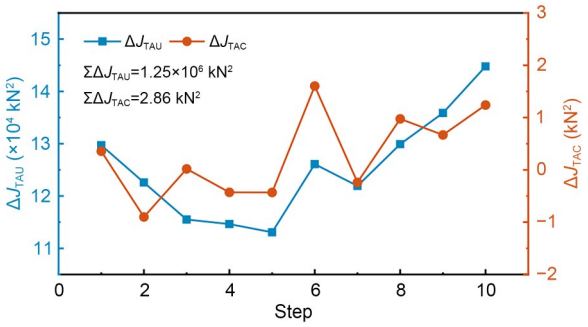

Fig. 7 Comparison between RTNFA and RTWFA

front consistently outperforms RTWFA in terms of force uniformity. In terms of the accumulated performance, RTNFA outperforms RTWFA by 1.25×10^6 kN^2 in force uniformity and 2.86 kN^2 in compliance. The accumulated value of ΔJ_{TAC} remains positive, even though it is not greater than zero at every time step. This demonstrates the superior overall compliance performance of RTNFA across the evaluation period. Moreover, it suggests that RTNFA is more adept at identifying viable force allocation methods within the feasible domain, which optimally balance uniformity and compliance. The results also reveal the limitations of the heuristic- and experience-based weighting methods in managing non-dominant relationships between the objectives, which frequently fail to produce a balanced solution. Conversely, the entropy-based weighting method enhances the efficiency of the 2D optimization by adaptively compensating for the changes in the data scale, thereby making the method more impartial.

5 Compromise for non-solution conditions

The feasible domain for force allocation in this study can be defined as an intersection of hyperplanes in 10D space. Under the constraints of the linear equations, a 7D affine subspace is obtained. The solution space is no longer a complete affine subspace once the hydraulic cylinder pressure limit is applied as a constraint in the feasible domain of QP. Instead, it is the intersection of the affine subspace and a higher-dimensional orthogonal half-space, creating a truncated high-dimensional convex polyhedron. Under certain strict constraints, it is likely that no intersection exists; that is, the feasible region is empty, and no solution can be found. For example, the feasible region corresponding to ring 96 is an empty set. However, RSDFA can find a solution if the lower bound of each group force is relaxed to zero. In most cases, this results in worse performance than FSDFA, as shown in Fig. 8. This is especially noticeable when RSDFA performs at its lowest value in the ramping-up stage, while it only progressively approaches FSDFA in the steady stage.

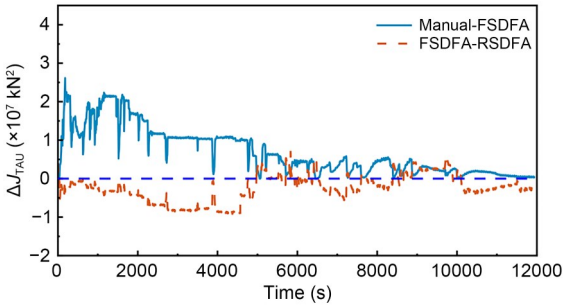

Fig. 8 Comparison of J_{TAU} in ring 96

Contrary to the previous result, this suggests that the region-reconfigurable approach has a detrimental effect on force uniformity in such cases. The fundamental cause of this is the geometric nature of the 7D affine subspace. The global optimum solution is located close to the boundary of the convex polytope. Thus, this method can only produce a suboptimal solution that is closest to the ideal point within the feasible region when the global optimum is unachievable. The forces in groups G to I are almost zero as shown in Fig. 9, and these areas correspond to the times when the RSDFA-to-FSDFA performance difference is negative. The QP-based force allocation method presented in this study is an equality-constrained convex optimization task. Therefore, the solution that QP identifies must be the best solution once the global optimum is located inside the feasible space.

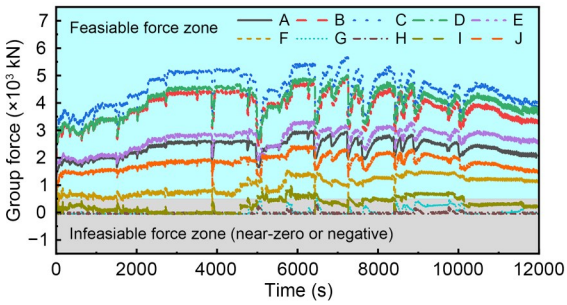

Fig. 9 Force of each group in ring 96

Nevertheless, unlike this convex optimization method, the GA does not rely on an unbiased and

closed-form representation of the feasible space. Instead, GA uses heuristic search techniques that either soften equality requirements into inequality constraints with tolerances or convert them into soft penalties. Therefore, even in cases when traditional solvers fail or the strict feasible area is empty, GA can estimate viable solutions. Three types of constraint–tolerance methods are currently in use with GA. The first one involves adjusting GA parameters to guide the search toward the feasible side of the solution space. However, this approach cannot leverage the knowledge from unfeasible solutions since it can only approximate the best solution from within the feasible domain. Therefore, in cases where QP has no solution, GA also tends to fail (theoretically) in finding a solution. The second type incorporates penalty terms in the fitness function, allowing unfeasible individuals to persist in the population. However, this method performs poorly when the feasible space occupies only a small fraction of the overall search space. The third type—which is only applicable when the constraints are relatively weak—turns the constraints into the objectives and solves the issue as an unconstrained multi-objective optimization problem.

Since the feasible solutions in these cases often lie close to the border of a high-dimensional convex polytope, we propose a hybrid method that combines GA with LLS. In particular, an initial solution is found using GA, which is treated as the initial guess to find the final solution that meets the stringent equality restrictions through LLS. This method leverages both the local convergence efficiency of LLS and the global search capability of GA. For situations where QP fails, the GA combined with LLS-based local force optimization (GLLFO) technique is promising.

Executing the GA involves initializing a population, evaluating fitness, selecting superior individuals, applying crossover to produce offspring, and using mutations to maintain diversity. Our application of the GA shares the same parameters as NSGA-II. The force allocation results are listed in Table 4. A subset of thrust force vector values from the above dataset was extracted for force allocation. The pitching moment M_y in step 4 deviated from the goal value by the greatest amount, 517.24 kN·m (or 2.11%). The operating principle of GLLFO is to sacrifice thrust force vector fitting accuracy in order to guarantee that high-level decisions always receive a corresponding solution. Thus, a timely response to the steering command is realized, thereby avoiding correction failures caused by unresponsiveness in the coordination layer. Moreover, the deviation remains within 3% of the desired thrust force vector, which is considered acceptable in practice. This is because the "Linghang" TBM employs the PPRV control mode, which uses a closed-loop pressure control method to realize trend-level displacement control (Zheng et al., 2024). Trend control does not impose strict requirements on the displacement tracking accuracy but instead requires that the resultant thrust force vector remain biased toward DTA. Therefore, if the moments M_x and M_y stay in the same quadrant and the advancing force F_z still satisfies the penetration requirement, the thrust system can successfully correct the trajectory even if the reconstructed thrust force vector deviates from the desired vector by about 3%.

6 Discussions

A pseudocode implementation for TS2DFA is provided in Section S3 of the ESM. When tunneling begins, the segment assembly position is entered to initiate a command that modifies the group layout. Real-time thrust force vectors are then gathered, and the force allocation strategy is determined by identifying the current tunneling stage. Once the TBM finishes the stable stage, the current allocation process is paused for segment installation. Afterwards, the K segment position is updated again, and the execution proceeds iteratively.

Choosing a suitable execution cycle is crucial for the force allocation framework, which is mainly

Table 4 Force allocation results of GLLFO

Step	Thrust force vector (kN, kN·m, kN·m)	J_{TAU} ($\times10^7$ kN^2)	Deviation (kN, kN·m, kN·m)
1	[3.88×10^4, 0.34×10^4, 2.33×10^4]	6.23	[-7.28×10^{-12}, -0.45×10^{-12}, -14.55×10^{-12}]
2	[3.89×10^4, 0.34×10^4, 2.38×10^4]	6.93	[71.92, 7.56, −76.21]
3	[3.90×10^4, 0.34×10^4, 2.42×10^4]	7.09	[259.46, 39.22, 226.30]
4	[3.88×10^4, 0.34×10^4, 2.45×10^4]	7.15	[483.09, 58.28, 517.24]

determined by the actuator delays. In practice, the delays can be divided into two parts: the response time of the hydraulic cylinders and the lag associated with the shield-ground interaction. The former arises because the two chambers of the hydraulic cylinders, the long pipelines, and the internal cavities of the valve blocks are all filled with compressible hydraulic oil. The refilling and compressing of the hydraulic oil results in a slow approach to the desired steady-state pressure. Moreover, the electro-mechanical inertia of the proportional valves, as well as of the accumulators and bypass leakage components, further prolongs the pressure settling time. The other part of the delay is caused by the interaction between the TBM and the surrounding ground. It can be abstracted as a multi-degree-of-freedom mass-spring damping system with very large inertia. Even after the hydraulic cylinder has reached the desired pressure, the newly constructed thrust force vector drives the TBM to move relative to the surrounding ground under its confinement. This involves compression and relaxation at the TBM-ground contact interface before an observable relative displacement occurs. Therefore, the measurable changes in TBM attitude inevitably lag behind adjustments to the force. These two delays are intrinsic physical properties of TBMs and cannot be eliminated. In practice, the on-site time delay needs to be measured and used as the period of force allocation. More details on the convergence properties of the proposed methods are shown in Section S4 of the ESM.

Notably, this approach can also be used in conjunction with the synchronized tunneling and segment assembly (STSA) mode of a TBM. When the tunneling states allow for the STSA, the thrust system switches to a working condition in which some hydraulic cylinders are temporarily deactivated. Most current research has adhered to the principle that the thrust force vector should remain constant before and after the cylinder retraction. However, considering the time variation of the thrust force vector during tunneling, the group forces must be adjusted in real time. Consequently, the execution still adheres to the process outlined in Section S4 of the ESM. The first distinction is that n_k, a_k, and b_k are defined differently depending on the number and locations of the retracted cylinders. Additionally, the two constraints must be changed as follows:

$$J_{\mathrm{TAU}} = \frac{1}{9}\sum_{k=1}^{9}(F_k - \bar{F})^2, \tag{17}$$

$$J_{\mathrm{TAC}} = \sum_{k=1}^{9}[F_k(m) - F_k(m-1)]^2. \tag{18}$$

Nonetheless, certain restrictions remain in terms of practical application. For one, it is uncommon for a multi-input, multi-output thrust system to simultaneously reach a steady state for each group. In general, some may have settled, while others may have not; therefore, the resulting thrust force vector will deviate from the decision-level objective during these brief intervals. Thus, the pressure-control response should be the primary focus of actual implementations that aim to address this problem. One approach is to utilize a feedforward or adaptive controller to make the pressures achieve a steady state more consistently, enabling the high-level decision to proceed more reliably. On the other hand, fuzzy logic-based multi-criteria decision making (MCDM) approaches have recently shown strong potential for handling linguistic, experience-based, or hard-to-quantify information. In this work, the evaluation indices (J_{TAU} and J_{TAC}) were computed directly from on-site sensor measurements and deterministic mechanical models. However, we hypothesize that the fuzzy MCDM method can be incorporated with force allocation when linguistic or experience-based information is required. For example, when geological risk levels are high (e.g., relatively soft, very weak, or heterogeneous interlayers), engineering judgments of segmental damage risk, or preferences on energy consumption or impact, can be integrated into the force allocation process in a fuzzy form. Thus, methods such as fuzzy technique for order preference by similarity to an ideal solution (TOPSIS) could be introduced as an upper-level decision module.

7 Conclusions

In this study, we propose a novel design for a region-reconfigurable thrust system for TBMs that dynamically modifies the group spatial arrangement based on the real-time position of the K segment. This arrangement successfully prevents cross-group force imbalances from producing overturning moments. Moreover, it offers greater flexibility in force allocation compared to the fixed-grouped thrust system, thereby

improving force uniformity throughout the segment ring. On this basis, a quasi-static equilibrium model under linear equality constraints is established, and two constraints are proposed accordingly: the force uniformity describes the variance in force among the groups and hydraulic compliance reflects the change in force over time.

During the ramping-up stage, only force uniformity is considered and optimized by the QP method. Field data demonstrated that FSDFA improved the force uniformity by 28.27% over the manual allocation results. Moreover, the improvement of force uniformity reaches up to 32.89% using RSDFA, confirming the theoretical advantage of convex optimization. Notably, for the majority of TBMs, even when using a fixed-grouped thrust system, there is usually only one PPRV for each hydraulic cylinder. By only allocating the group force to the appropriate PPRVs, this region-reconfigurable method can be implemented directly without the need for hardware modification.

As for the steady stage—where the hydraulic compliance also becomes a concern—two constraints are optimized simultaneously. The final solution is obtained using NSGA-II and TOPSIS. The results indicate that the weighted gradient direction of QP may deviate from the desired outcome in the 10D solution space, resulting in worse performance than NSGA-II. Moreover, we present a novel solver that combines GA and LLS to overcome the infeasibility associated with strict constraints. GLLFO can ensure that the high-level decisions are always correct, at the cost of a 3% deviation between the presented thrust force vector and the expected one. More significantly, the thrust system is not the only possible application for this force allocation framework. With appropriate modification of the constraints and equations, it could easily be applied to other parallel subsystems in TBM, such as the cutterhead driving system. This highlights its versatility and potential for broader deployment in future intelligent TBM systems.

Acknowledgments

This work is supported by the National Key Research and Development Program of China (No. 2022YFC3802302) and the National Natural Science Foundation of China (No. 52475075).

Author contributions

Conceptualization: Zhe ZHENG and Dong HAN; methodology: Zhe ZHENG and Kaihao ZHU; software: Jiaqi HOU and Fulong LIN; validation: Laikuang LIN; formal analysis: Zhe ZHENG; investigation: Zhe ZHENG and Haibo XIE; data curation: Lianhui JIA; writing–original draft preparation: Zhe ZHENG and Lijie JIANG; writing–review and editing: Zhe ZHENG and Kaihao ZHU; visualization: Zhe ZHENG and Jiaqi HOU; project administration: Huayong YANG; funding acquisition: Dong HAN. All authors have read and agreed to the published version of the manuscript.

Conflict of interest

Huayong YANG is an Editor-in-Chief of this journal, and is NOT involved in the editorial review or the decision to publish this article. Zhe ZHENG, Kaihao ZHU, Jiaqi HOU, Haibo XIE, Lijie JIANG, Fulong LIN, Lianhui JIA, Laikuang LIN, Huayong YANG, and Dong HAN declare that they have no conflict of interest.

References

Chen JS, Mo HH, 2009. Numerical study on crack problems in segments of shield tunnel using finite element method. *Tunnelling and Underground Space Technology*, 24(1): 91-102. https://doi.org/10.1016/j.tust.2008.05.007

Chen K, Yang YD, 2017. Innovation and development trends of shield manufacturing technology in China. *Tunnel Construction*, 37(3):276-284 (in Chinese). https://doi.org/10.3973/j.issn.1672-741X.2017.03.003

Dai ZY, Li PN, Wang X, et al., 2022. Asymmetric force effect and damage analysis of unlooped segment of large-diameter shield under synchronous propulsion and assembly mode. *Applied Sciences*, 12(6):2850. https://doi.org/10.3390/app12062850

Deng KS, Huang JL, Wang HG, 2015. Layout optimization of non-equidistant arrangement for thrust systems in shield machines. *Automation in Construction*, 49:135-141. https://doi.org/10.1016/j.autcon.2014.10.006

Deng KS, Li YY, Zhang XM, et al., 2021. Optimal layout design for thrust systems in earth pressure balance shield machines under sudden loads. *Arabian Journal for Science and Engineering*, 46(3):2793-2802. https://doi.org/10.1007/s13369-020-05269-w

Deng KS, Tang XQ, Wang LP, et al., 2011a. Force transmission characteristics for the non-equidistant arrangement thrust systems of shield tunneling machines. *Automation in Construction*, 20(5):588-595. https://doi.org/10.1016/j.autcon.2010.11.025

Deng KS, Tang XQ, Wang LP, et al., 2011b. Research on characteristics of deformation in thrust system for EPB shield machines. *Tunnelling and Underground Space Technology*, 26(1):15-21. https://doi.org/10.1016/j.tust.2010.06.008

Deng KS, Yin ZR, Meng BL, et al., 2019. A load-balancing-oriented symmetrical uneven layout design for thrust system in tunneling machines under composite ground. *Proceedings of the Institution of Mechanical Engineers, Part C: Journal of Mechanical Engineering Science*, 233(8):

2847-2854.
https://doi.org/10.1177/0954406218791639

Elbaz K, Shen SL, Zhou AN, et al., 2024. Reinforcement learning-based optimizer to improve the steering of shield tunneling machine. *Acta Geotechnica*, 19(6):4167-4187.
https://doi.org/10.1007/s11440-023-02136-4

Gong J, Bao TF, Zhu Z, et al., 2024. BIM-based framework of automatic tunnel segment assembly and deviation control. *Underground Space*, 16:59-78.
https://doi.org/10.1016/j.undsp.2023.09.005

Guo K, Xu YP, Li JF, 2018. Thrust force allocation method for shield tunneling machines under complex load conditions. *Automation in Construction*, 96:141-147.
https://doi.org/10.1016/j.autcon.2018.08.016

Guo WT, Guo WZ, 2017. A novel self-adaptive thrust system of shield machine under complex geological working condition. *Tunnelling and Underground Space Technology*, 63:133-143.
https://doi.org/10.1016/j.tust.2016.12.017

Harandizadeh H, Armaghani DJ, Asteris PG, et al., 2021. TBM performance prediction developing a hybrid ANFIS-PNN predictive model optimized by imperialism competitive algorithm. *Neural Computing and Applications*, 33(23):16149-16179.
https://doi.org/10.1007/s00521-021-06217-x

Hu M, Wu BJ, Zhou WB, et al., 2022. Self-driving shield: intelligent systems, methodologies, and practice. *Automation in Construction*, 139:104326.
https://doi.org/10.1016/j.autcon.2022.104326

Jia GP, Huo JZ, Yang BW, et al., 2023. The real-time optimal attitude control of tunnel boring machine based on reinforcement learning. *Applied Sciences*, 13(18):10026.
https://doi.org/10.3390/app131810026

Kong XX, Tang L, Ling XZ, et al., 2024. Development of shield model test system for studying the bias load of shield in soil-rock compound strata. *Tunnelling and Underground Space Technology*, 143:105464.
https://doi.org/10.1016/j.tust.2023.105464

Li JB, Chen ZY, Li X, et al., 2023a. Feedback on a shared big dataset for intelligent TBM Part I: feature extraction and machine learning methods. *Underground Space*, 11:1-25.
https://doi.org/10.1016/j.undsp.2023.01.001

Li JB, Chen ZY, Li X, et al., 2023b. Feedback on a shared big dataset for intelligent TBM Part II: application and forward look. *Underground Space*, 11:26-45.
https://doi.org/10.1016/j.undsp.2023.01.002

Li ZM, Yazdani Bejarbaneh B, Asteris PG, et al., 2021. A hybrid GEP and WOA approach to estimate the optimal penetration rate of TBM in granitic rock mass. *Soft Computing*, 25(17):11877-11895.
https://doi.org/10.1007/s00500-021-06005-8

Lin PH, Wu MZ, Xiao ZH, et al., 2024. Physics-informed deep reinforcement learning for enhancement on tunnel boring machine's advance speed and stability. *Automation in Construction*, 158:105234.
https://doi.org/10.1016/j.autcon.2023.105234

Liu XY, Shao C, 2010. Present status and prospect of shield machine automatic control technology. *Journal of Mechanical Engineering*, 46(20):152-160 (in Chinese).
https://doi.org/10.3901/JME.2010.20.152

MMC-Gamuda Tunnelling Training Academy, 2020. Tunnelling | Malaysia's Self Driving TBMs.
https://www.newcivilengineer.com/innovative-thinking/tunnelling-malaysias-self-driving-tbms-18-02-2020/

Shi CH, Wang ZX, Gong CJ, et al., 2022. Prediction of the additional structural response of segmental tunnel linings induced by asymmetric jack thrusts. *Tunnelling and Underground Space Technology*, 124:104471.
https://doi.org/10.1016/j.tust.2022.104471

Shi H, Gong GF, Yang HY, et al., 2013. Compliance of hydraulic system and its applications in thrust system design of shield tunneling machine. *Science China Technological Sciences*, 56(9):2124-2131.
https://doi.org/10.1007/s11431-013-5248-8

SASAC (State-owned Assets Supervision and Administration Commission of the State Council), 2023. Shanghai's First Subway Using Self Driving Shield Technology Successfully Launched (in Chinese).
http://www.sasac.gov.cn/n2588025/n2588129/c28677934/content.html

Tang L, Kong XX, Ling XZ, et al., 2022. Deviation correction strategy for the earth pressure balance shield based on shield-soil interactions. *Frontiers of Mechanical Engineering*, 17(2):20.
https://doi.org/10.1007/s11465-022-0676-4

Wang JY, 2017. Super-large diameter shield tunneling technologies in China in recent decade. *Tunnel Construction*, 37(3):330-335 (in Chinese).
https://doi.org/10.3973/j.issn.1672-741X.2017.03.011

Wang S, Zhang YK, Gong GF, 2024. Optimal decision-making system of shield tunneling parameters based on LSTM and MNSGA-II. Proceedings of 2024 IEEE International Conference on Automatic Control and Intelligent Systems, p.65-70.
https://doi.org/10.1109/I2CACIS61270.2024.10649853

Wang XY, Yuan DJ, Jin DL, et al., 2022. Determination of thrusts for different cylinder groups during shield tunneling. *Tunnelling and Underground Space Technology*, 127:104579.
https://doi.org/10.1016/j.tust.2022.104579

Xu H, Zhou J, Asteris PG, et al., 2019. Supervised machine learning techniques to the prediction of tunnel boring machine penetration rate. *Applied Sciences*, 9(18):3715.
https://doi.org/10.3390/app9183715

Xu J, Bu JF, Zhang LG, et al., 2023. Intelligent decision framework of shield attitude correction based on deep reinforcement learning. Proceedings of the 17th East Asian-Pacific Conference on Structural Engineering and Construction, p.1273-1287.
https://doi.org/10.1007/978-981-19-7331-4_102

Yang YB, Zhou B, Xie XY, et al., 2018. Characteristics and causes of cracking and damage of shield tunnel segmented lining in construction stage—a case study in Shanghai soft soil. *European Journal of Environmental and Civil Engineering*, 22(sup1):s213-s227.
https://doi.org/10.1080/19648189.2017.1356243

Zhang YK, Gong GF, Yang HY, et al., 2020. Precision versus

intelligence: autonomous supporting pressure balance control for slurry shield tunnel boring machines. *Automation in Construction*, 114:103173. https://doi.org/10.1016/j.autcon.2020.103173

Zhang YK, Gong GF, Yang HY, et al., 2022. Towards autonomous and optimal excavation of shield machine: a deep reinforcement learning-based approach. *Journal of Zhejiang University-SCIENCE A*, 23(6):458-478. https://doi.org/10.1631/jzus.A2100325

Zhang YK, Gong GF, Yang HY, et al., 2024. From tunnel boring machine to tunnel boring robot: perspectives on intelligent shield machine and its smart operation. *Journal of Zhejiang University-SCIENCE A*, 25(5):357-381. https://doi.org/10.1631/jzus.A2300377

Zheng Z, Luo KD, Tan XZ, et al., 2024. Autonomous steering control for tunnel boring machines. *Automation in Construction*, 159:105259. https://doi.org/10.1016/j.autcon.2023.105259

Zhu YT, Zhai YX, Min R, et al., 2021. Model test on the synchronous technology combining with shield tunneling and segment assembling based on the linear distribution principle of the thrust force. *IOP Conference Series*: *Earth and Environmental Science*, 861:052079. https://doi.org/10.1088/1755-1315/861/5/052079

Zhu YT, Zhu YF, Chen EJ, et al., 2023. Synchronous shield tunnelling technology combining advancement and segment fabrication: principle, verification and application. *Underground Space*, 13:23-47. https://doi.org/10.1016/j.undsp.2023.03.003

Electronic supplementary materials

Sections S1–S4